Neural Network-based Single-carrier Joint Communication and Sensing: Loss Design, Constellation Shaping and Precoding

CHARLOTTE MUTH[1]**, (Graduate Student Member, IEEE), BENEDIKT GEIGER**[1]**, (Graduate Student Member, IEEE), DANIEL GIL GAVIRIA**[1]**, (Graduate Student Member, IEEE), and LAURENT SCHMALEN**[1]**, (Fellow, IEEE)**

[1]Communications Engineering Lab (CEL), Karlsruhe Institute of Technology (KIT), Hertzstr. 16, 76187 Karlsruhe, Germany

Corresponding author: Charlotte Muth (e-mail: muth@kit.edu).

ABSTRACT We investigate the impact of higher-order modulation formats on the sensing performance of single-carrier joint communication and sensing (JCAS) systems. Several separate components such as a beamformer, a modulator, a target detector, an angle of arrival (AoA) estimator and a communication demapper are implemented as trainable neural networks (NNs). We compare geometrically shaped modulation formats to a classical quadrature amplitude modulation (QAM) scheme. We assess the influence of multi-snapshot sensing and varying signal-to-noise ratio (SNR) on the overall performance of the autoencoder (AE)-based system. To improve the training behavior of the system, we decouple the loss functions from the respective SNR values and the number of sensing snapshots, using upper bounds of the sensing and communication performance. The NN-based sensing outperforms classical algorithms, such as a Neyman-Pearson based power detector for object detection and ESPRIT for AoA estimation for both the trained constellations and QAM at low SNRs. We show that the gap in sensing performance between classical and shaped modulation formats can be significantly reduced through multi-snapshot sensing. Lastly, we demonstrate system extension to multi-user multiple-input multiple-output (MIMO) to address the improvement of spatial efficiency when servicing multiple user equipments (UEs). Our contribution emphasizes the importance of estimation bounds for training neural networks, especially when the trained solutions are deployed in varying SNR conditions.

INDEX TERMS Joint communication and sensing, Neural networks, Angle estimation, Object detection, Higher-order modulation formats, 6G

I. INTRODUCTION

Digital communication is a vital service for our hyper-connected society. The integration of a sensing service, which aids automotive vehicles to detect potential collisions or enables finer beam alignment, could improve the user experience of mobile network users. An increase in spectral and energy efficiency can be achieved by combining radio communication and sensing into one waveform instead of operating two separate systems. Therefore, this work focuses on the codesign of both functionalities in a joint communication and sensing (JCAS) system. The future 6G network is expected to natively support JCAS by introducing object detection of objects without communication capabilities and by performing general sensing of the surroundings [2]. With this approach, we expect to increase the spectral efficiency by providing spectral resources for sensing while maintaining their use for communication, as well as the energy efficiency because of the dual use of a joint waveform.

There is growing interest in data-driven solutions based on machine learning (ML) since they can overcome deficits such as hardware impairments, faced by algorithms derived using model-based techniques [3]. Especially at higher carrier frequencies, which will become more important in 6G, these deficits become more pronounced due to hardware imperfections [4]. ML is expected to be prevalent in 6G, as its use in communication and radar signal processing has matured in

recent years [2].

For a communication-centric JCAS network, it is essential to first guarantee communication capabilities. Therefore, the effects of transmit signal design, such as the choice of modulation formats, are of particular interest. Many studies such as [5], [6] showcase sensing using only phase modulation, however, higher-order QAM formats are often employed in legacy communication systems to increase throughput and reliability.

In this paper, we study the monostatic sensing capabilities of a wireless communication system with multiple snapshots. We consider single-carrier modulation to reduce the computational complexity of the simulations. Our findings can generally be transferred to multi-carrier systems such as orthogonal frequency-division multiplexing (OFDM). Our contributions are:

- We compare an autoencoder (AE)-based geometric constellation shaping approach to classical QAM to analyze in detail the impact on communication and sensing in different signal-to-noise ratio (SNR) environments and multi-snapshot sensing.
- We modify the loss function for the end-to-end training to improve training over a wide range of SNR conditions
- We show that the loss modification improves the angle of arrival (AoA) estimation and that the detection and communication loss terms do not profit from modification.
- We extend the AE-approach to demonstrate servicing multiple user equipments (UEs).

The remainder of this paper is structured as follows: Section II introduces the proposed system model. In Sec. III, the design and training of the deep neural networks (DNNs) are described. Section IV presents the results of the simulations performed, including evaluation of bit-wise mutual information (BMI), root mean squared error (RMSE) of angle estimation, detection rate, and false alarm rate for object detection. Lastly, in Sec. VI, we conclude this work.

A. RELATED WORK

ML approaches allow the joint optimization of the transmitter and receiver taking into account sensing and communications performance metrics. AEs have been studied as a promising ML approach for communication systems [7], [8], and for radar [9], [10] independently of each other. As JCAS has gained significant attention within the scientific community, ML research for JCAS has emerged, merging approaches for radar and communications. In [3], an AE for JCAS in a single-carrier system has been proposed, performing close to a maximum a posteriori ratio test detector benchmark for single snapshot sensing of one radar target. In [11], this approach was extended to multiple targets, addressing the problem of target matching. The work of [4] extends these methods to an OFDM waveform using model-based learning, which is a well-known technique to combine communication and radar [12], [13]. These works demonstrate the potential of deep-learning-based sensing to mitigate hardware mismatches.

However, the research has been limited to single snapshot estimation. We presented an extension to multiple-snapshot sensing in [1], while limiting ourselves to QAM modulation. In this work, we demonstrate the effect of constellation shaping and give a detailed analysis of our approach.

B. NOTATION

$\mathbb{R}$ and $\mathbb{C}$ denote the set of real and complex numbers, respectively. Sets are generally denoted by calligraphic font, e.g., $\mathcal{X}$, with the cardinality of a set being $|\mathcal{X}|$. We denote vectors and matrices with boldface lowercase and uppercase letters, e.g., vector $\boldsymbol{x}$ and matrix $\boldsymbol{X}$. The single matrix element in the nth row and the kth column of the matrix $\boldsymbol{X}$ is denoted as x_{nk}. The transpose and conjugate transpose of a matrix $\boldsymbol{X}$ are written as $\boldsymbol{X}^\top$ and $\boldsymbol{X}^H$, respectively, while the Hadamard product is indicated with the operator $\odot$ and the outer product with the operator $\otimes$. The diagonal matrix $\boldsymbol{D}$ with diagonal entries $\boldsymbol{d}$ is denoted as $\mathrm{diag}(\boldsymbol{d})$ and the all-one column vector of length N is denoted as $\mathbf{1}_N$. A complex normal distribution with mean μ and variance σ^2 is denoted as $\mathcal{CN}(\mu, \sigma^2)$. Random variables are denoted with sans-serif font, e.g. x, with multivariate random variables x, mutual information $I(\mathsf{x}_1, \mathsf{x}_2)$, entropy $H(\mathsf{x})$ and cross-entropy $H(\mathsf{x}_1 || \mathsf{x}_2)$.

II. SYSTEM MODEL

In this paper, we investigate a monostatic JCAS setup, where the transmitter and the sensing receiver are co-located, e.g., part of the same base station, and have multiple antennas. Our goal is to detect a target and estimate its AoA θ based on the reflection of the transmitted signal at the potential target. The transmit signal is simultaneously used to communicate with a UE with a single antenna at a different position than the sensing target. The UE is located randomly at an azimuth angle $\varphi \in [\varphi_{\min}, \varphi_{\max}]$ and the radar target is located randomly at an azimuth angle of $\theta \in [\theta_{\min}, \theta_{\max}]$. In the considered scenario, the communication area $[\varphi_{\min}, \varphi_{\max}]$ and sensing area $[\theta_{\min}, \theta_{\max}]$ do not overlap. We consider multi-snapshot sensing with N_{win} samples to provide more detailed information on the sensing targets. The system block diagram is illustrated in Fig. 1. The blocks shaded in blue are trainable neural networks (NNs) and the following subsections explain in detail the signal processing of the system.

A. TRANSMITTER

A modulator with $M = 2^c$, $c \in \mathbb{N}$ different modulation symbols transforms the data symbols $m \in \{1, 2, \ldots, M\}$ into complex symbols $x \in \mathcal{M} \subset \mathbb{C}$, where $\mathcal{M}$ contains the M distinct modulation symbols. The transmitter generates a sequence of cN_{win} independent and identically distributed random bits that are transformed into a vector $\boldsymbol{x} \in \mathbb{C}^{N_{\mathrm{win}}}$ through a fixed bit mapping for blockwise processing. Each bit vector $\boldsymbol{b} = (b_1, \ldots, b_c)^\top \in \{0, 1\}^c$ is mapped to a unique symbol x.

The transmitter is equipped with K antennas and uses digital precoding, i.e., a unique complex factor $v_k = g_k \exp(\mathrm{j}\vartheta_k)$ is generated for each antenna $k \in \{1, 2, \ldots, K\}$ with am-
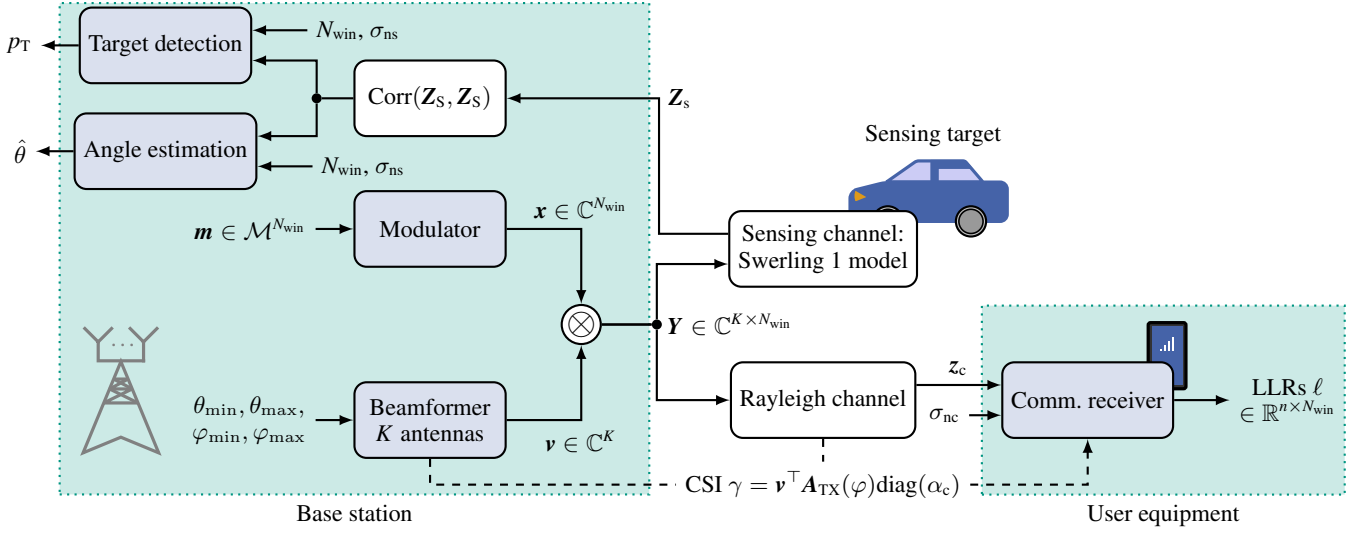
FIGURE 1. JCAS system, light blue blocks are trainable NNs. The modulator can be implemented as an NN or with a classical QAM constellation.

plitude g_k and phase shift ϑ_k to steer the signal to a certain area of interest. The beamformer is implemented as an NN and has the limits of the azimuth angle regions in which communication and sensing should take place, i.e., $\{\varphi_{\min}, \varphi_{\max}, \theta_{\min}, \theta_{\max}\}$ as inputs. The use of an NN enables analysis of an optimized power trade-off between the sensing and communication functionality. The output of the NN is a vector $\boldsymbol{v} \in \mathbb{C}^K = (v_1, v_2, \ldots, v_K)^\top$ containing the complex factors of each antenna. The modulator and beamformer employ power normalization to meet power constraints.

The transmit signal $\boldsymbol{Y} \in \mathbb{C}^{K \times N_{\text{win}}}$ is the outer product of the complex modulation symbols $\boldsymbol{x}$ and the beamformer output $\boldsymbol{v}$. Specifically, $\boldsymbol{Y}$ can be expressed as

$$\boldsymbol{Y} = \boldsymbol{v} \otimes \boldsymbol{x}. \tag{1}$$

B. CHANNELS

A part of the radiated power is steered toward the communication receiver by the beamformer while another part is reflected by the object of interest and reaches the sensing receiver co-located with the transmitter. The signal propagation from K antennas towards the object located at an azimuth angle φ_i is modeled with the spatial angle matrix $\boldsymbol{A}_{\text{TX}}(\varphi) = (\boldsymbol{a}_{\text{TX}}(\varphi_1) \ldots \boldsymbol{a}_{\text{TX}}(\varphi_{N_{\text{win}}})) \in \mathbb{C}^{K \times N_{\text{win}}}$ whose columns are given by

$$\boldsymbol{a}_{\text{TX}}(\varphi) = \left(1, \mathrm{e}^{\mathrm{j}\pi \sin \varphi}, \ldots, \mathrm{e}^{\mathrm{j}\pi (K-1) \sin \varphi}\right)^\top, \tag{2}$$

assuming the antenna spacing matches exactly $\lambda/2$ of the transmission wavelength λ.

For communications, we consider the UE at a different uniformly distributed angle for each communication sample to generate varied training data. The signal $\boldsymbol{Y}$ experiences a single-tap Rayleigh fading channel before being received by the UE with a single antenna as

$$\boldsymbol{z}_{\text{c}} = \boldsymbol{1}_K^\top \left(\boldsymbol{A}_{\text{TX}}(\varphi) \odot \boldsymbol{Y}\right) \mathrm{diag}(\alpha_{\text{c}}) + \boldsymbol{n}_{\text{c}}^\top, \tag{3}$$

with channel coefficient $\alpha_{\text{c},n} \sim \mathcal{CN}(0, \sigma_{\text{c}}^2)$ and noise samples $n_{\text{c},n} \sim \mathcal{CN}(0, \sigma_{\text{nc}}^2)$. We select a constant $\varphi_i \in [\varphi_{\min}, \varphi_{\max}]$ uniformly at random during an observation window N_{win} to analyze multi-snapshot sensing and define $\text{SNR}_{\text{c}} = \sigma_{\text{c}}^2/\sigma_{\text{nc}}^2$. The total SNR is corrected with the beamforming gain β_{c} to $\text{SNR} = \beta_{\text{c}} \cdot \text{SNR}_{\text{c}}$.

With $T \in \{0, 1\}$ indicating the presence of a potential target, we express the sensing signal reflected from said target in the monostatic setup as

$$\boldsymbol{Z}_{\text{s}} = T \boldsymbol{a}_{\text{RX}}(\theta) \boldsymbol{a}_{\text{TX}}(\theta)^\top \boldsymbol{Y} \mathrm{diag}(\alpha_{\text{s}}) + \boldsymbol{N}_{\text{S}}, \tag{4}$$

with the radar target following a Swerling-1 model [14] with $\alpha_{\text{s},n} \sim \mathcal{CN}(0, \sigma_{\text{s}}^2)$ representing radar cross section and path loss and $\boldsymbol{N}_{\text{s}}$ consisting of noise samples $n_{\text{s},nk} \sim \mathcal{CN}(0, \sigma_{\text{ns}}^2)$. The spatial angle vectors relate as $\boldsymbol{a}_{\text{RX}}(\theta) = \boldsymbol{a}_{\text{TX}}(\theta)$, with θ being the AoA of the target throughout the observation window N_{win}. With a Swerling-1 model, we model scan-to-scan deviations of the radar cross section (RCS), which manifest as a change in $\alpha_{\text{s},n}$ during N_{win}. The radial velocity of the target is assumed to be zero, so no Doppler shift occurs.

C. SENSING RECEIVER

The sensing receiver, which is part of the base station, detects the potential target and estimates its AoA using a linear array of K antennas. We consider multiple snapshot sensing with N_{win} snapshots, enabled by forming the short-term spatial auto-correlation of all considered samples across the receive antennas defined as

$$\text{Corr}(\boldsymbol{Z}_{\text{s}}, \boldsymbol{Z}_{\text{s}}) := \frac{1}{N_{\text{win}}} \boldsymbol{Z}_{\text{s}} \boldsymbol{Z}_{\text{s}}^H \quad \in \mathbb{C}^{K \times K}. \tag{5}$$

This metric approximates a sufficient statistic for AoA estimation and detection as outlined in Appendix B. Next,

$$C_{\mathrm{CR}}(\theta) = \frac{1}{\pi^2 \cos(\theta)^2} \frac{\sigma_{\mathrm{ns}}^2}{2N_{\mathrm{win}}} \left(\mathrm{Re} \left\{ \left[\beta_{\mathrm{s}} \sigma_{\mathrm{s}}^2 \left[\frac{K \beta_{\mathrm{s}} \sigma_{\mathrm{s}}^2}{\sigma_{\mathrm{ns}}^2 + K \beta_{\mathrm{s}} \sigma_{\mathrm{s}}^2} \right] \right] \cdot \frac{K^3 - K}{12} \right\} \right)^{-1} \tag{6}$$

$\mathrm{Corr}(\mathbf{Z}_{\mathrm{s}}, \mathbf{Z}_{\mathrm{s}})$ and N_{win}, and $\sigma_{\mathrm{n,s}}$ are passed to the target detection and angle estimation blocks which are implemented as NNs and described in Sec. III. The target detection block outputs a probability $p_{\mathrm{T}} \in [0, 1]$ which denotes the certainty that a target is present ($T = 1$). The angle estimation block outputs $\hat{\theta} \in [-\frac{\pi}{2}, \frac{\pi}{2}]$, which indicates the estimated azimuth AoA of the target.

D. COMMUNICATION RECEIVER

At the communication receiver, our goal is to recover the transmitted bits based on the received signal, i.e., demodulate the received signal. The communication receiver is implemented as a NN that outputs log-likelihood ratios (LLRs) $\ell \in \mathbb{R}^{n \times N_{\mathrm{win}}}$ that can be used as input to a soft decision channel decoder. For the demodulation, we assume that channel estimation has already been performed at the communication receiver and that the precoding matrix $\mathbf{v}$ is known. Therefore, channel state information (CSI) $\gamma = \mathbf{v}^\top \mathbf{A}_{\mathrm{TX}}(\varphi) \mathrm{diag}(\alpha_{\mathrm{c}})$ is available at the communication receiver. It is important to note that this CSI has no effect on the sensing functionality of the system.

E. PERFORMANCE INDICATORS

We formulate bounds on the communication throughput and estimation accuracy as theoretical performance indicators for the system.

1) Constellation Kurtosis

In [15], it was shown that the random-deterministic sensing trade-off for OFDM-sensing can be controlled by the kurtosis, i.e., the fourth standardized moment of the constellation, if a matched filter is applied to estimate the sensing channel. As OFDM sensing and AoA estimation are both harmonic retrieval problems, these findings can be reapplied to our scenario. The constellation kurtosis is directly connected to the achievable detection rate in sensing. The kurtosis is not directly linked to the communication performance. Nevertheless, the kurtosis constraint places restrictions on constellation design and can affect achievable data rates. Assuming equal symbol probability, we use the mean minimum distance $\bar{d}_{\mathrm{min}}$ defined as

$$\bar{d}_{\mathrm{min}} = \frac{1}{|\mathcal{M}|} \sum_{x_m \in \mathcal{M}} \min_{x_n \in \mathcal{M} \setminus \{x_m\}} |x_n - x_m| \tag{6}$$

as an indicator for the communication performance and relate it to the kurtosis of a constellation. Typically, a larger $\bar{d}_{\mathrm{min}}$ leads to a smaller bit error rate (BER), especially for pragmatic constellation diagrams where the spacing between neighboring constellation points is similar for all constellation symbols.
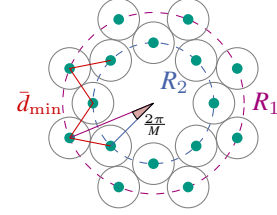

FIGURE 2. Example constellation of APSK to explore performance for constellations with different kurtosis

To demonstrate the relationship between the minimum distance $\bar{d}_{\mathrm{min}}$ and the kurtosis κ, we design an amplitude phase shift keying (APSK) as a constellation using two 8 phase shift keyings (PSKs) on radii R_1 and R_2 with an offset phase of $\frac{2\pi}{M}$ between the constellation points on circle R_1 and R_2 as shown in Fig. 2. The APSK allows a continuous evaluation of the kurtosis.

Then, $R_1 = \sqrt{2 - R_2^2}$ is obtained by power normalization and the kurtosis κ of the constellation with mean $\mu_{\mathcal{M}} = 0$ and standard deviation $\sigma_{\mathcal{M}} = 1$ follows as

$$\kappa = \frac{1}{|\mathcal{M}|} \sum_{m \in \mathcal{M}} \left| \frac{x_m - \mu_{\mathcal{M}}}{\sigma_{\mathcal{M}}} \right|^4 = \frac{R_1^4 + R_2^4}{2}. \tag{7}$$

The minimum distance follows from trigonometric identities as

$$\bar{d}_{\mathrm{min}} = \sqrt{2 - 2\sqrt{\kappa} \cos\left(\frac{2\pi}{M}\right)}, \tag{8}$$

which is valid for $\bar{d}_{\mathrm{min}} \leq 2R_2 \sin\left(\frac{2\pi}{M}\right)$, i.e., until the inner circle becomes too small to fit an 8PSK with point distance of at least $\bar{d}_{\mathrm{min}}$. This constellation yields an achievable relationship between kurtosis and mean minimum distance for this specific constellation topology without claiming optimality.

2) Cramér-Rao Bound

The adaptation of the Cramér-Rao bound (CRB) to the designed system is derived in Appendix A. For the estimation of the angle of a single target, the CRB amounts to (6), where N_{win} is the number of samples collected, θ the angle to be estimated, β the beamforming gain, and K the number of antennas [16]. The given CRB is a lower bound for the variance of an unbiased estimator.

3) Bit-wise Mutual Information

Although a blockwise processing is indicated in Fig. 1 with block length N_{win}, we consider the statistics of single modulation symbols for evaluation (as the channel is memoryless). The aim of the communication receiver is to maximize the BMI, since transmission uses bit-interleaved coded modulation (BICM) and forward error correction (FEC) to enable

reliable communication. The BMI is therefore used as a surrogate measure for communication performance after FEC without the need to consider a specific coding approach in this work. Maximizing the BMI is equivalent to minimizing the binary cross entropy (BCE) between true bit labels b_i and the estimated bit labels $\hat{b}_i$ [8, Eq. (8)]:

$$\text{BMI} = \sum_{i=1}^{\log_2 M} I(b_i; z_c) \qquad (7)$$

$$= H(b) - \sum_{i=1}^{\log_2 M} H(b_i || \hat{b}_i)$$

$$+ \sum_{i=1}^{\log_2 M} \mathbb{E}_\gamma \left[D_{\text{KL}}(p(b_i|z_c) || p(\hat{b}_i|z_c)) \right], \quad (8)$$

with source entropy $H(b)$, binary cross-entropy $H(b_i||\hat{b}_i)$ and the expected Kullback-Leibler divergence D_{KL} that denotes the expected mismatch of the true posterior $p(b_i|z_c)$ given the observed receiver signal and the approximated (by the receiver) posterior $p(\hat{b}_i|z_c)$ over different channel realizations. The BMI is an achievable rate using binary coding and pragmatic coded modulation.

III. NEURAL NETWORK TRAINING AND VALIDATION
A. NEURAL NETWORK CONFIGURATION
Our system is configured similarly to that of [11]. Function blocks such as beamforming, target detection, angle estimation, demapping and optionally modulation are implemented as separate NNs. The NN layer dimensions are given in Tab. 1. The NNs consist of fully connected layers with ELU activation function in the hidden layers.

We implement modulation as a classical QAM and for comparison as a trainable NN. Inputs are symbol indices with a known fixed bit mapping. The inputs of the beamformer are the areas of interest for sensing $\{\theta_{\min}, \theta_{\max}\}$ and for communication $\{\varphi_{\min}, \varphi_{\max}\}$. The output of the transmitter is subject to power normalization.

At the communication receiver, miminum mean squared error (MMSE) equalization is performed, compensating for the complex random channel tap, to achieve better convergence along different SNR values. The outputs of the communication receiver are interpreted as LLRs for each bit. For the BER calculation, we use the hard decision of these LLR values. As stated in Sec. II, we strive to improve the performance for multiple snapshot estimation by calculating the short-term spatial auto-correlation matrix (ACM) $\text{Corr}(\mathbf{Z}_s, \mathbf{Z}_s)$. The number of input neurons of the sensing receiver is $K^2 + 2$. Two input neurons have N_{win} and σ_{ns} as inputs and allow the investigation of sensing for varying channel parameters. Specifically, our systems are trained for generalized N_{win} and σ_{ns}, allowing flexible investigation within the range of training parameters. This parameterization leads to roughly the same communication and sensing performance as systems trained individually for different N_{win} and σ_{ns}, while allowing flexible operation without requiring a change of the NN

TABLE 1. Sizes of neural networks

Component	Input layer	Hidden layers	Output
Beamformer	4	$\{K, K, 2K\}$	$2K$
Demapper	3	$\{10M, 10M, 10M, 10M\}$	$\log_2(M)$
Angle estimation	$2K^2 + 2$	$\{8K, 4K, 4K, K\}$	1
Detection	$2K^2 + 2$	$\{2K, 2K, K\}$	1
Modulator	M	$\{8M, 8M, 8M\}$	2

weights and, at the same time reducing the computational complexity required for training.

During training, a vector indicating the presence of a target is fed to the sensing receiver in order to calculate the detection threshold that is needed to keep the false alarm rate P_f constant. This threshold is added to the output of the detection NN before applying the output sigmoid function. Since this threshold is numerically calculated for each system, there are small variations expected. The output function of the angle estimation NN is $\frac{\pi}{2}\tanh(\cdot)$, normalizing the output to $\pm\frac{\pi}{2}$.

B. LOSS FUNCTIONS
There are three main components of the loss function, resulting in a multi-objective optimization, which evaluates the performance of communication, detection, and angle estimation. We introduce a weight $w_s \in [0, 1]$ that controls the impact or perceived importance of the sensing tasks, resulting in the full loss term

$$L = (1 - w_s)L_{\text{comm}} + w_s L_{\text{detect}} + w_s L_{\text{angle}}. \qquad (9)$$

JCAS systems have been trained in [11] with N different scenarios where a target is present using the loss given by

$$L = (1 - w_s)\underbrace{\sum_{i=1}^{\log_2 M} H(b_i || \hat{b}_i)}_{L_{\text{comm}}}$$

$$+ w_s \left(\underbrace{H(t||\hat{t})}_{L_{\text{detect}}} + \underbrace{\frac{1}{N}\sum_{i=1}^{N}(\theta_i - \hat{\theta}_i)^2}_{L_{\text{angle}}} \right). \qquad (10)$$

When training multiple functionalities and multiple operating scenarios simultaneously, we observed a reduced performance when using (10) as a loss function. Especially the AoA estimation showed unreliable convergence. The achievable precision, which is bounded by (6), depends significantly on the chosen N_{win} and σ_{ns}. After training, the estimator should yield a mean squared error (MSE) similar to the lower bounds, i.e., the CRB, of the estimator. The lower bound is not constant in all training scenarios, since it depends on N_{win} and σ_{nc} resulting in a perturbation of the loss. Therefore, we introduce bound-informed adaptations to ensure a robust performance over a range of SNRs and observation window lengths N_{win}. We expect increased precision and better convergence behaviour if the loss is normalized across multiple SNRs and N_{win}.

The CRB is used for an informed modification of the loss function used for the training of NNs. Under the assumption of $\sigma_{ns}^2 \ll K\beta\sigma_s^2$, we simplify (6) to separate the expression into parts depending on N_{win} and σ_{ns}:

$$C_{CR}(\theta) \approx \frac{1}{\pi^2 \cos(\theta)^2} \frac{\sigma_{ns}^2}{N_{win}} \frac{1}{\beta_s \sigma_s^2} \frac{6}{K^3 - K}. \quad (11)$$

The factor σ_{ns}^2 / N_{win} describes the impact of the observation window and SNR on the bound. Therefore, we modify the loss term with the correction factor N_{win}/σ_{ns}^2. The proposed loss term is then given by

$$L_{angle} = \frac{1}{N} \sum_{i=1}^{N} \frac{N_{win,i}}{\sigma_{ns,i}^2} (\theta_i - \hat{\theta}_i)^2, \quad (12)$$

achieving loss terms with similar magnitude for varying N_{win} and σ_{ns} and regularizing the output.

There are multiple examples for training communication systems over varying SNRs [8], [17]; but a gradient perturbation or problems during training have not been reported. To complete our analysis of loss behaviour, we consider the behaviour of BCE for our channel model and varying N_{win} and SNRs. In the following, we show why a modification of the communication loss term is not necessary. We adapt the communication loss that is evaluated based on the known bits $b_{i,n}$, with i denoting the bit in a specific symbol and n denoting the symbol index, and estimated bits $\hat{b}_{i,n}$ based on output probabilities $p(\hat{b}_{i,n} = 1|z_c) = \sigma(\ell_{i,n})$, with $\sigma(\cdot)$ being the sigmoid function and the output LLRs $\ell_{i,n}$. Traditionally, the BCE $H(b||\hat{b})$ is used as a loss function, given by

$$\sum_{i=1}^{\log_2 M} H(b_i||\hat{b}_i) = -\sum_{i=1}^{\log_2 M} b_i \log_2(p(\hat{b}_i = 1|z_c))$$
$$+ (1 - b_i) \log_2(1 - p(\hat{b}_i = 1|z_c)). \quad (13)$$

Assuming independent bits, the BCE and BMI are related as [8]

$$\sum_{i=1}^{\log_2 M} H(b_i||\hat{b}_i) = H(b) - BMI$$
$$+ \sum_{i=1}^{\log_2 M} \mathbb{E}_\gamma \left[D_{KL}(p(b_i|z_c)||p(\hat{b}_i|z_c)) \right]. \quad (14)$$

We lower bound the BCE as

$$\sum_{i=1}^{\log_2 M} H(b_i||\hat{b}_i) \overset{(a)}{\geq} H(b) - I(b; z_c)$$
$$+ \sum_{i=1}^{\log_2 M} \mathbb{E}_\gamma \left[D_{KL}(p(b_i|z_c)||p(\hat{b}_i|z_c)) \right] \quad (15)$$

$$\overset{(b)}{\geq} H(b) - I(b; z_c) \quad (16)$$

$$\overset{(c)}{\geq} H(b) - C, \quad (17)$$

where in (a), we upper bound the BMI by the mutual information $I(b; z_c)$. The Kullback-Leibler divergence $D_{KL} \geq 0$ describes the mismatch of the true posterior distributions and the distributions at the NN output. With converged systems, this mismatch should be very small, encouraging us to drop the term in (b). Finally, we bound the mutual information by the channel capacity C in (c).

The ergodic channel capacity C for a Rayleigh fading channel is given by $C_e = \log_2\left(1 + \frac{\sigma_c^2 \cdot \bar{\beta}_c P_s}{\sigma_{nc}^2}\right)$ [18], with $\bar{\beta}_c$ denoting the average beamforming gain for the area of interest for communication. For a single realization, $I(b; z_c)$ could be larger than the ergodic capacity, but considering many different realizations for a loss function and the law of large numbers diminish this possibility. Then

$$\sum_{i=1}^{\log_2 M} H(b_i||\hat{b}_i) \gtrapprox H(b) - \log_2\left(1 + \frac{\sigma_c^2 \bar{\beta}_c P_s}{\sigma_{nc}^2}\right) \quad (18)$$

$$= H(b) - \log_2\left(\underbrace{\sigma_{nc}^2 + \sigma_c^2 \bar{\beta}_c P_s}_{\sigma_{nc}^2 \ll \sigma_c^2 \bar{\beta}_c P_s}\right)$$
$$+ \log_2\left(\sigma_{nc}^2\right) \quad (19)$$

$$\approx H(b) - \log_2\left(\sigma_c^2 \bar{\beta}_c P_s\right) + \log_2\left(\sigma_{nc}^2\right). \quad (20)$$

The approximation in (20) is valid for high SNR. In lower SNR scenarios, the BCE is underestimated when using (20). Based on (20), the terms $\log_2\left(\sigma_c^2 \bar{\beta}_c P_s\right)$ describes the impact of the beamforming while the term $\log_2\left(\sigma_{nc}^2\right)$ represents the impact of SNR variations which we aim to remove from the loss. A loss function modification following our arguments for (12) results in:

$$L_{comm} = \frac{-1}{N \log_2 M} \sum_{i=1}^{N} \left(\sum_{k=1}^{\log_2 M} \left(b_{i,k} \cdot \log_2(p(\hat{b}_{i,k} = 1|z_{c,i})) \right. \right.$$
$$\left. \left. + (1 - b_{i,k}) \cdot \log_2(p(\hat{b}_{i,k} = 0|z_{c,i})) \right) + \log_2(\sigma_{nc,i}^2) \right). \quad (21)$$

This loss function can be used for optimization of the various NN-based blocks using the Adam optimizer [19]; therefore, the gradients of L_{comm} with respect to the weights of the neural networks are used for optimization. However, since the offset term $\log_2(\sigma_{nc,i}^2)$ in (21) is additive and does not depend on the weights, its gradient will be zero and will not affect the training. Hence, it can be omitted from (21), which then boils down to the BCE loss, showing that modification of the BCE loss for communication is not necessary.

For the detection loss, we can use the same approach of modifying the BCE between the true presence of targets $t \in \{0, 1\}^N$ and the detection output p_T, keeping in mind that the SNR scales with $\sqrt{N_{win}}$:

$$H(t||\hat{t}) \approx H(t) - \log_2\left(\sigma_s^2 \bar{\beta}_s P_s\right) + \log_2\left(\frac{\sigma_{ns}^2}{\sqrt{N_{win}}}\right). \quad (22)$$

We can derive a loss similar to (21), given by

$$
L_{\text{detect}} = \frac{-1}{N} \sum_{i=1}^{N} \mathsf{t}_i \cdot \log_2(p_\mathrm{T}) + (1 - \mathsf{t}_i) \cdot \log_2(1 - p_\mathrm{T}) \\
+ \log_2\left(\frac{\sigma_{\text{ns},i}^2}{\sqrt{N_{\text{win},i}}} \right). \tag{23}
$$

With the same arguments as given before, the last term $\log_2\left(\frac{\sigma_{\text{ns},i}^2}{\sqrt{N_{\text{win},i}}} \right)$ does not impact the training behavior. Therefore, a modification of the BCE as loss term for communication and object detection is not necessary for the described system configuration.

Furthermore, we want to ensure a constant false alarm rate P_f over different SNRs and observation window lengths N_{win}. The input of the detection NN is normalized to $\text{Corr}(\mathbf{Z}_\mathrm{s}, \mathbf{Z}_\mathrm{s})/\sigma_{\text{ns},i}^2$ to obtain the same noise statistic and, therefore, false alarm rates for different SNRs. We apply different decision thresholds for each window length N_{win} that are calculated numerically after training the NN components, explained in Sec. III-C.

C. NEURAL NETWORK TRAINING

The training comprises three phases: Pre-training, fine-tuning, and limiting. In pre-training, the detection and angle estimation neural network are trained independently, i.e., the other loss terms of Eq. 9 are set to 0. We use a total of $2.5 \cdot 10^7$ communication symbols for both pre-training steps, divided into mini-batches of 10^4 symbols. We use the Adam optimizer with a learning rate of 10^{-4}. The length of the sensing window is randomly and uniformly chosen between 1 and 15 for each sensing state, to generalize to different N_{win} and to give insight into multi-snapshot behavior. Fine-tuning establishes the operating point of the JCAS trade-off. The fine-tuning is performed on $5 \cdot 10^7$ symbols by using the whole loss function in (9) starting with the parameters established in the pre-training. We use the same hyperparameters as used for pre-training. Lastly, limiting ensures that the constant false alarm rate is maintained. In the limiting phase, the system runs separately for 10^4 symbols for each length of the sensing window N_{win}. The neural network components are not trained anymore in this phase, but the decision threshold for detection is refined as described in [11].

For validation of the communication component, we choose the BMI and BER as metrics. The BMI represents the maximum number of bits per symbol that can be reliably transmitted on average with the given system.

The object detection task is evaluated on the basis of its detection rate and false alarm rate. For direct comparison, we design detectors with a constant false alarm rate.

The AoA estimation is evaluated on the RMSE of angle estimates. We evaluate the AoA on all the present targets instead of only on the detected targets as in [3].

IV. SIMULATION RESULTS AND DISCUSSION

In our simulations, the communication receiver is located at an AoA of $\varphi \in [30°, 50°]$. Radar targets are found in a range $\theta \in [-20°, 20°]$. Our monostatic transmitter and sensing receiver are both simulated as a linear array with 16 antennas and we consider an observation window up to $N_{\text{win}} = 15$ and modulation with $M = 16$. For the radar receiver, our objective is to achieve a false alarm rate of $P_\mathrm{f} = 10^{-2}$ while optimizing the detection rate and angle estimator.

A. BENCHMARKS FOR MODULATION, DETECTION AND ANGLE ESTIMATION

We train NNs to optimize the modulation format as in [11], enabling geometric constellation shaping, and compare it to a classical QAM to quantify the gains of the optimized constellation.

For detection, we employ a generalized power detector based on a Neyman-Pearson (NP) criterion [16, Chap. 10] as a benchmark, distinguishing between two normal distributions of mean 0 with different variances. The exact transmit sequence $\mathbf{X}$ as well as prior knowledge about the sensing area are not available. In the reference detector, the average power of all the input samples $z_{\text{s},il}$ considered for sensing is computed. The detector can be formulated as
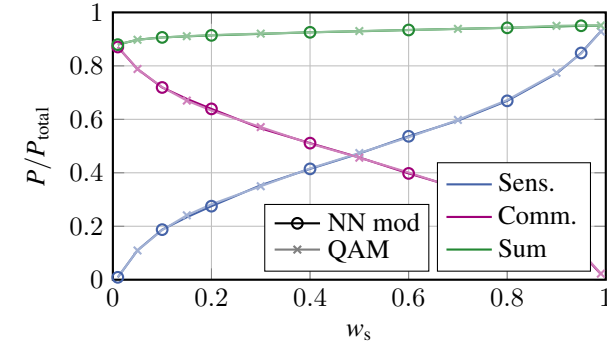
$$
\frac{2}{\sigma_{\text{ns}}^2} \sum_{l=1}^{N_{\text{win}}} \sum_{i=1}^{K} |z_{\text{s},il}|^2 \underset{\hat{t}=0}{\overset{\hat{t}=1}{\gtrless}} \chi_{2KN_{\text{win}}}^2(1 - P_\mathrm{f}), \tag{24}
$$

where $\chi_{2KN_{\text{win}}}^2(\cdot)$ denotes the density of the chi-squared distribution with $2KN_{\text{win}}$ degrees of freedom. The correction factor is caused by the transformation of the problem from complex to real numbers, therefore artificially doubling the number of samples but reducing the noise variance by a factor of $\sqrt{2}$. The benchmark detector has a constant false alarm rate along varying values of SNR_s and N_{win}.
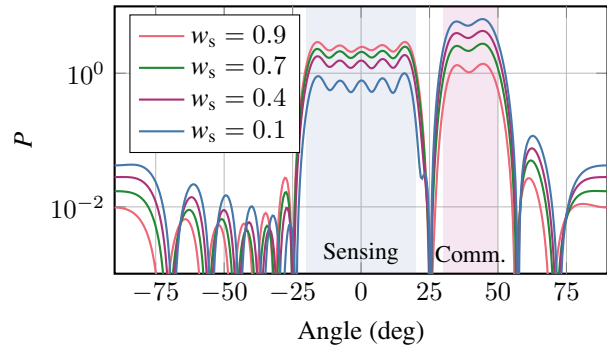
We use the well-studied ESPRIT algorithm as a benchmark for angle estimation as presented in [16]. ESPRIT performs close to the CRB for high SNRs or large observation window length N_{win}.

B. BEAMFORMING RESULTS

In Fig. 3(a), we show the effect of the trade-off parameter w_s on the power radiated to the different areas of interest. The power distribution for a system using QAM is identical to a system with a shaped constellation. At $w_\mathrm{s} = 0.5$, the power is almost equally distributed to the sensing and the communication functionality. For $w_\mathrm{s} < 0.2$ and $w_\mathrm{s} > 0.8$, the power radiated toward the less favored function decreases more rapidly. The sum of the radiated power in both areas of interest increases slightly with increasing w_s, but approximately 10% of the total power is radiated outside of our areas of interest. In Fig. 3(b), the beam patterns for selected values of w_s are shown. We radiate more power outside our area of interest while prioritizing communication, which is caused by higher side lobes, particularly at an angle of $\pm 90°$. We also observe a slight widening of the communication beam for

(a) Power distribution for areas of interest

(b) Beam pattern outputs for QAM, areas of interests are shaded

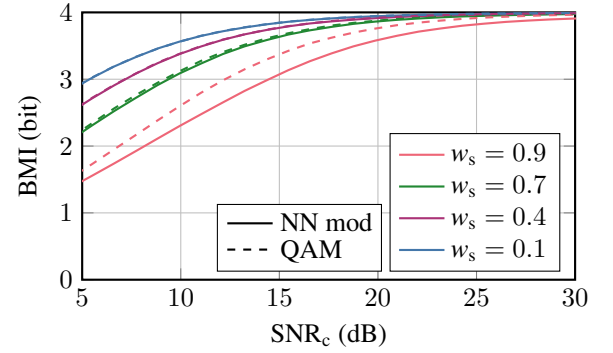**FIGURE 3.** Beamforming results for different operating points w_s

decreasing w_s, which contributes to higher emissions outside our areas of interest.
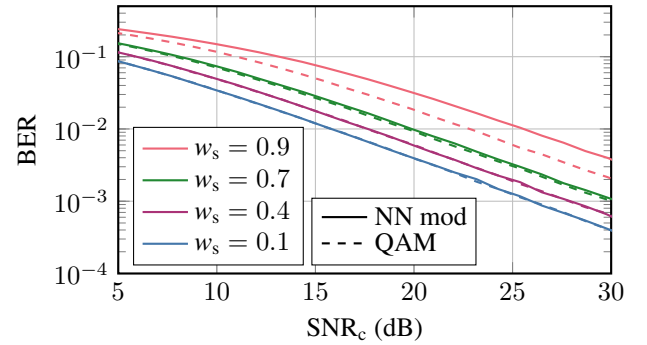
C. COMMUNICATION RESULTS

In Fig. 4(a), we show the BMI for different w_s values. As $M = 16$, the BMI cannot exceed 4 and slowly saturates to this level for high SNR. The shaped constellations perform very close to QAM for $w_s \geq 0.7$. Fig. 4(b) displays the BER over a range of SNR values and different trade-off factors w_s. We observe, as expected, that the BER increases for higher w_s. Two main effects are responsible for this degradation: Part of the BER degradation can be attributed to the shaped constellation diagrams, while the rest is attributed to the beamforming gain toward the communication receiver. We can directly observe the degradation caused by the beamforming gain considering QAM in Fig. 4(b). Since the same QAM is used for all w_s, the performance gap is caused by the beamforming gain only. We can see that QAM performs robustly over the different SNR values. The QAM results experience an SNR offset when varying w_s, since the beamforming gain varies for different w_s. For $w_s \leq 0.7$, the performance of the shaped constellation and QAM are nearly identical.

In Fig. 4(c), we can verify that the trained detectors for QAM perform very close to the MLD. The SNR is normalized by beamforming gain $\bar{\beta}_c$ for comparability.
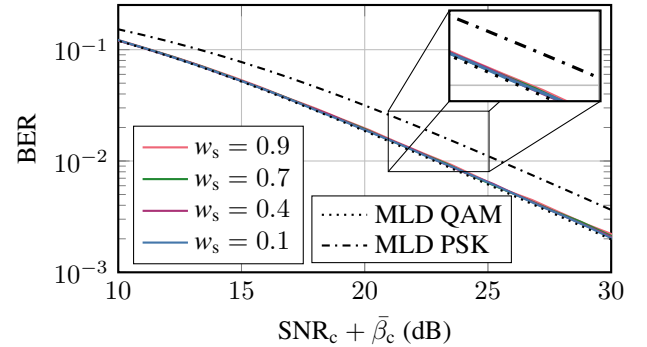
The performance degradation caused by the shaped constellations can be quantified using Fig. 4(d), where the SNR is corrected with the beamforming gain, enabling a raw compar-
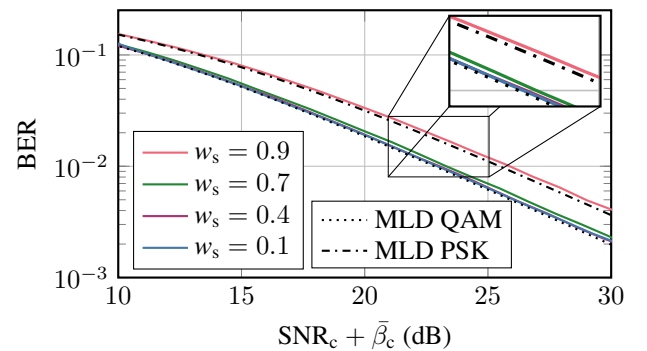

(a) BMI after training NN modulator vs QAM for different w_s

(b) BER after training NN modulator vs QAM

(c) Trained system using QAM compared to maximum likelihood demapper (MLD) for QAM and PSK

(d) Trained system using shaped constellation compared to MLD for QAM and PSK

FIGURE 4. Comparison of communication performance of systems using QAM or constellation shaping
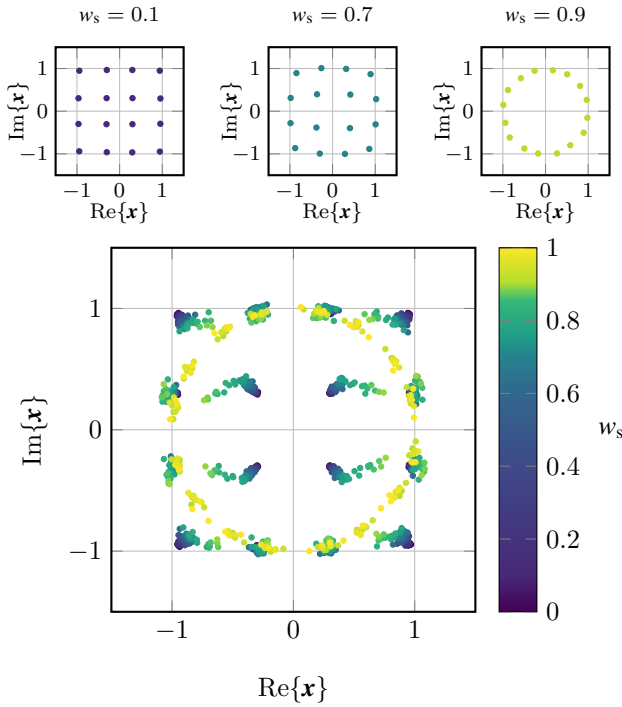
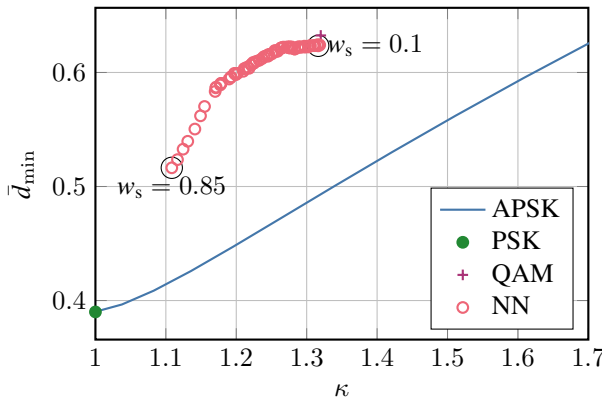**FIGURE 5.** Constellation evolution with w_s for SNR$_c$ = 20 dB

FIGURE 6. Communication performance evaluated based on the mean minimum distance between constellation points and the kurtosis κ

ison of the performance caused by changing the constellation. For comparison, we also show the MLD results for conventional 16-QAM and 16-PSK in Fig. 4(d). We can observe a performance close to the MLD for all trained systems. As expected, the performance for low w_s is close the MLD for QAM, but for $w_s = 0.9$ we observe a performance penalty of approximately 0.4 dB to the MLD for PSK.

Depending on the priority of the communication quality set by w_s and the channel SNR, different constellations are obtained, as shown in Fig. 5. In particular, if the sensing priority is very low, the constellation diagram resembles a

QAM[1]. When the priority of the sensing task increases, the inner symbols are slowly pushed outwards. At very high sensing priority ($w_s \approx 1$), the constellation resembles a PSK-like constellation, as the transmit power becomes equal over all symbols, resulting in a constant modulus signal. This indicates the importance of the kurtosis or a constant modulus constraint for JCAS systems. As the constellation converges to a constant amplitude with increasing w_s, communication becomes less reliable since the Euclidean distance between the constellation symbols becomes smaller.

Finally, in Fig. 6, we show the effect of the constellation kurtosis on the mean minimum distance $\bar{d}_{\min}$ by comparing the geometrically shaped constellations obtained from the NN to the APSK proposed in Sec. II-E1, a QAM and a pure PSK. As expected, a higher kurtosis allows the constellation points to be spaced further apart, resulting in a higher $\bar{d}_{\min}$ and a lower BER eventually. The reference APSK clearly shows this relationship between the kurtosis and the mean minimum distance $\bar{d}_{\min}$ in Fig. 6. The $\bar{d}_{\min}$ of the trained constellations is higher than the $\bar{d}_{\min}$ of the APSK. With decreasing w_s, the kurtosis κ and the $\bar{d}_{\min}$ increase, approaching the $\bar{d}_{\min}$ of a QAM. Especially for higher-order modulation formats, the kurtosis κ manifests as an additional trade-off parameter for sensing and communication performance.

D. TARGET DETECTION RESULTS
In Fig. 7(a), we compare the performance of the trained detectors at varying SNR. $\tilde{P}_f$ is approximately constant at 10^{-2}, as intended by design. The detection rate is very similar for both modulation methods, only for high w_s, we can see a slightly better detection rate for the shaped constellation. We converge to $\tilde{P}_d \approx 1$ for all cases. The impact of beamforming is clearly visible, especially for very low w_s, where the beamformer barely illuminates the sensing area and $\tilde{P}_d = 0.5$ is obtained only at SNR$_s$ = 2 dB. In Fig. 7(b), we correct for the average beamforming gain and observe that most detectors converge to a very similar performance. In Fig. 7(c) the trained detectors are shown with the benchmark NP-based detectors. All NN-based detectors trained for QAM perform almost identically and we can observe a reduced detection rate of the NP-based power detectors.

We evaluate target detection by comparing the detection rate $\tilde{P}_d$ and the false alarm rate $\tilde{P}_f$ for different observation window lengths N_{win} for $w_s = 0.9$ in Fig. 8. Increasing N_{win} improves the detection rate, as expected. The false alarm rate remains approximately constant for varying N_{win}. The NP benchmark detector leads to a lower detection rate for both setups, since it only relies on the input power. The trained detector can also take directional information into account.

Having reviewed the effects of multi-snapshot estimation and the use of different modulation formats, the presented setups enables us to choose different trade-offs between communication and sensing. Even though we sacrifice some

---

[1] If the BER is optimized instead of symbol error rates, QAM shows better performance than hexagonal lattices, as effective Gray coding in a hexagonal lattice is not possible
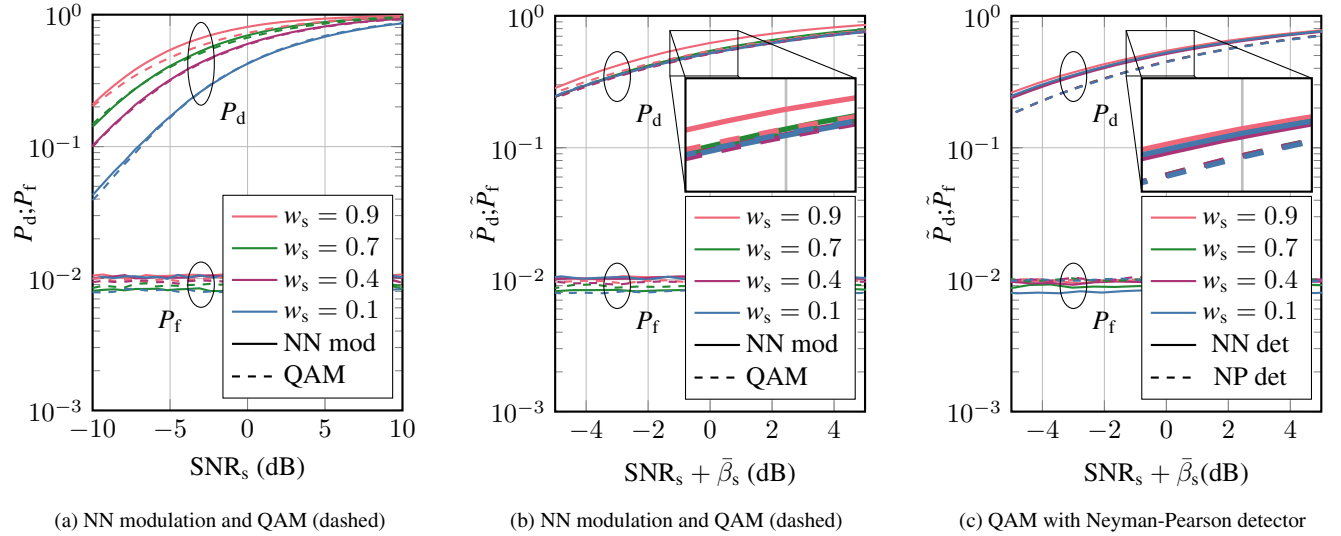
(a) NN modulation and QAM (dashed) (b) NN modulation and QAM (dashed) (c) QAM with Neyman-Pearson detector

FIGURE 7. Detection probability and false alarm rate for varying SNR and single snapshot detection
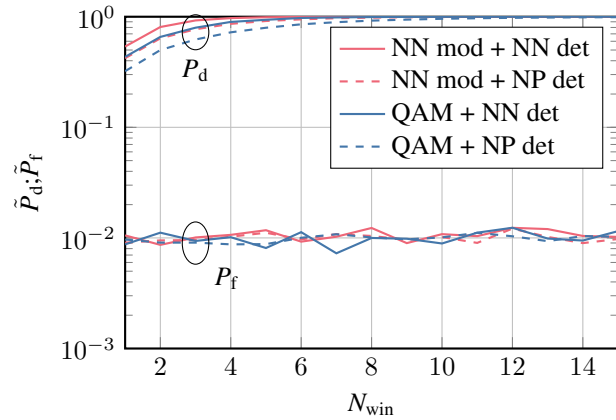

FIGURE 8. NN modulation and QAM with Neyman-Pearson benchmark, $\text{SNR}_s = -5$ dB, $w_s = 0.9$
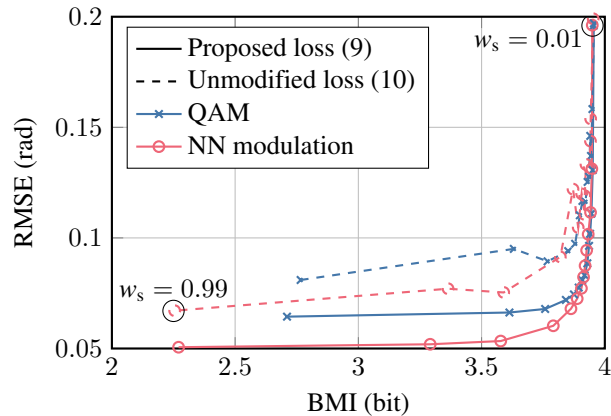

FIGURE 9. QAM and NN modulator operating at different w_s after training with the modified loss function (solid) and without (dashed). Performance evaluated at $\text{SNR}_c = 20.8$ dB, $\text{SNR}_s = 2.6$ dB and $N_{\text{win}} = 1$

sensing performance through the use of QAM, we can significantly improve detection and parameter estimation by collecting multiple samples to perform sensing in scenarios where objects are slow enough to be captured by multiple samples at almost the same position.

E. ANGLE ESTIMATION RESULTS

We analyze the effect of the modified angle loss term on the results compared to the unmodified loss given in (10) in Fig. 9. We optimize the JCAS system by choosing different trade-off factors w_s and display the RMSE of the angle of estimation as a function of the BMI for each value of w_s. With the original loss function (10), as indicated by the dashed lines, there are performance fluctuations. After training, the estimation error depends mainly on the noise power and N_{win}. Since N_{win} and σ_{ns} are randomly chosen during training, the loss is influenced by random processes which distort the magnitude of the gradients. Nevertheless, this randomness during training is beneficial for generalization. During training, we also noticed that trained systems converged to solutions of varying performance. We would anticipate a monotonic behavior of the curves, from high w_s in the left bottom corner of the plot to low w_s in the upper right corner. By modifying the loss function, we keep the randomness in our training data while normalizing the expected magnitude of the gradients. We achieve a gradual performance trade-off as expected and achieve a lower AoA estimation RMSE than for the unmodified loss while a similar BMI is achieved. The trained constellation generally achieves better accuracy in estimating the AoA, which can be attributed to its smaller constellation kurtosis.

We investigate the estimation bias of the AoA NN in Fig. 10(a). The trained estimators lead to small biases in the order of 10^{-2}. There is not a clear trend of the bias as a function of SNR or w_s, or a systematic bias. In Fig. 10(b), we
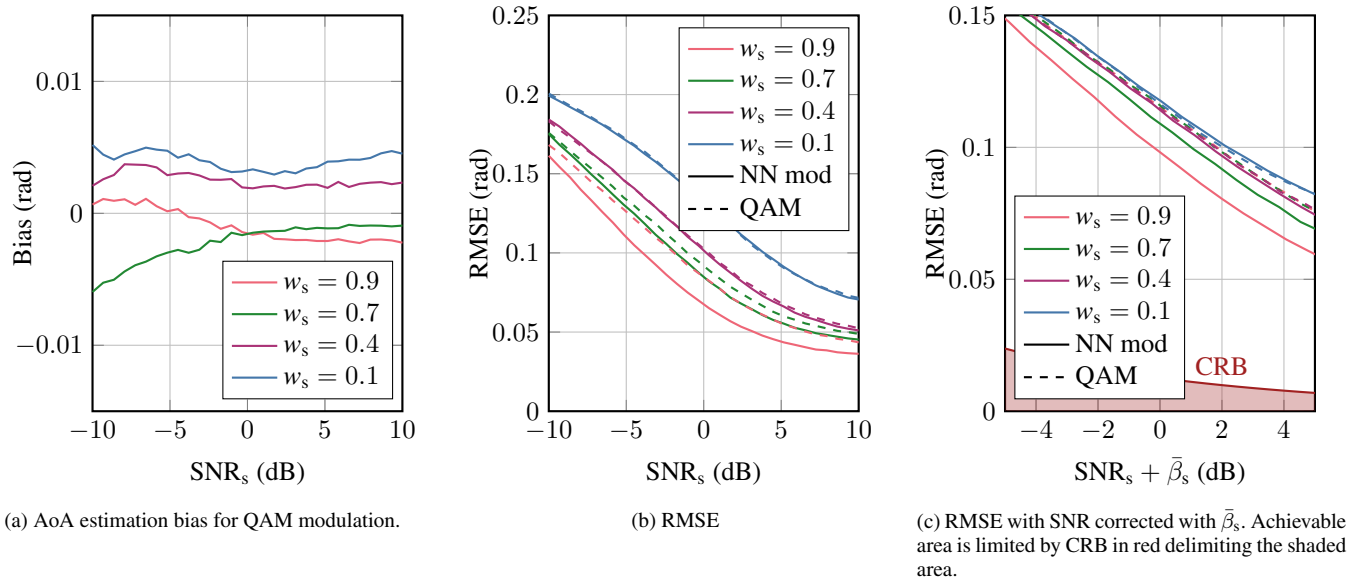
(a) AoA estimation bias for QAM modulation.

(b) RMSE

(c) RMSE with SNR corrected with $\bar{\beta}_s$. Achievable area is limited by CRB in red delimiting the shaded area.

FIGURE 10. AoA estimation results evaluated on different SNR for single snapshot sensing
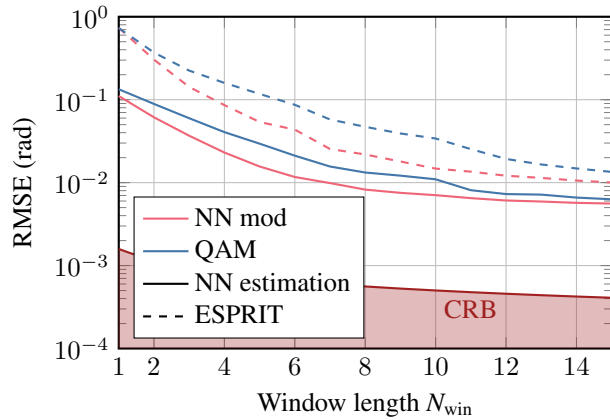

FIGURE 11. RMSE of angle estimation compared to ESPRIT algorithm for QAM and NN-based modulation at an SNR of -5 dB for the sensing channel with $w_s = 0.9$. Achievable area is limited by CRB.

can observe how increasing w_s decreases the angle estimation error. In particular, while the changes of BER for $w_s = 0.7$ in Fig. 4(b) between trained constellation and QAM are not very distinct, there is a gain in sensing performance. From Fig. 10(c), we can observe that for larger w_s, the gap of NN modulation and QAM increases further. Furthermore, as the priority of sensing is very low for $w_s = 0.1$, the sensing does not approach the results of the other detectors for QAM. We know from Fig. 3(b) that at $w_s = 0.1$, the beam towards the sensing targets varies in magnitude in our area of interest more significantly than for higher w_s, indicating that the minima in the wider beam lead to a high RMSE for targets. in Fig. 11, we compare different window lengths N_{win}. The trained angle estimators outperform ESPRIT at a raw SNR$_s = -5$ dB. At low SNR, the proposed method can consistently outperform the ESPRIT baseline. The gap between the modulation formats first becomes larger with increasing window length until $N_{\text{win}} \approx 4$ for both modulation methods. Since both modulators lead to the same average output power,

a longer observation window reduces the variance of the autocorrelation, under the assumption of a similar statistic for both modulation formats. There is a gap to the CRB for all estimators as expected in such a low SNR scenario.

V. SCENARIO EXTENSION: MULTI-USER MIMO

We extend the analyzed scenario to the downlink of multi-user multiple-input multiple-output (MIMO), to demonstrate how spatial efficiency can be addressed with our setup. In this section, we show a proof-of-concept how to extend the system of Fig. 1 to N_{ue} UEs. The beamforming NN needs to be extended to enable precoding for multiple different positions, therefore we enlarge the output layer to $2K \cdot N_{\text{ue}}$ neurons. The inputs of the precoding NN are then $\{\varphi_{\min}, \varphi_{\max}, \theta_{\text{ue}1}, \ldots, \theta_{\text{ue}N_{\text{ue}}}\}$ and (1) is replaced by

$$Y = V \cdot X, \qquad (25)$$

with $V \in \mathbb{C}^{K \times N_{\text{ue}}}$ being the precoding matrix and $X \in \mathbb{C}^{N_{\text{ue}} \times N_{\text{win}}}$ denoting the transmit symbols for all UEs.

We need to use a different loss term for communication to address the resource allocation. We reformulate the maximization of an α-fair utility function or the weighted sum rate as in [20, (5)] to a loss function as

$$\tilde{L}_{\text{comm}}(\alpha) =$$
$$\begin{cases} -\sum_{n=1}^{N_{\text{ue}}} \log_2 \left(\sum_{i=1}^{\log_2 M} \left[1 - H(\mathsf{b}_{i,n} || \hat{\mathsf{b}}_{i,n}) \right] \right) & , \alpha = 1 \\ -\sum_{n=1}^{N_{\text{ue}}} \frac{\left(\sum_{i=1}^{\log_2 M} \left[1 - H(\mathsf{b}_{i,n} || \hat{\mathsf{b}}_{i,n}) \right] \right)^{1-\alpha}}{1-\alpha} & , \alpha \neq 1, \end{cases}$$
$$(26)$$

with $\alpha \in \mathbb{R}^+$ trading off the total throughput and fairness between UEs. $\alpha = 0$ results in a sum-rate maximization and $\alpha = 1$ yields maximum fairness. Fairness is especially important in scenarios, where the channel capacities between UE and the base station vary significantly between UEs to prevent UEs with low channel capacity from being allocated
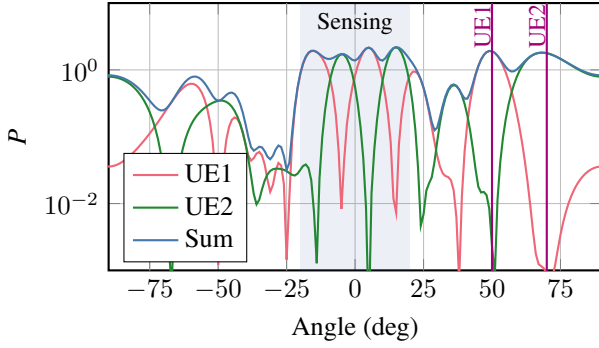
FIGURE 12. Beam patterns outputs for two UEs using QPSK in the multi-user MIMO scenario
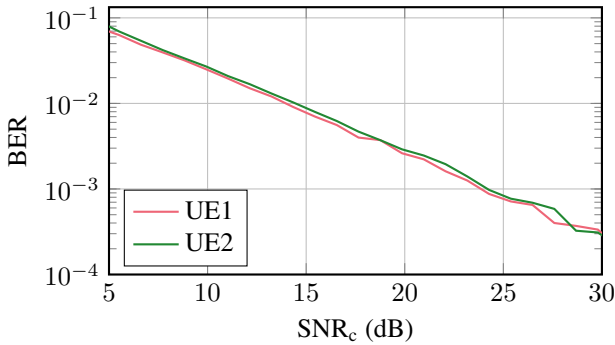

FIGURE 13. BER for 2 UEs for different SNRs using QPSK for modulation and the beam patterns of Fig. 12

no resources at all. In our training setup, $\tilde{L}_{\text{comm}}(\alpha)$ replaces L_{comm} in (9).

We demonstrate such a system with 2 UEs whose dominant reflection path is at an angle of departure of $50°$ and $70°$ respectively. The simulated SNR range is the same for both UEs and we train a respective decoder while QPSK is used for transmission. This setup results in the same total data throughput as the other simulations in this paper. Both UEs attempt to receive the same number of symbols. For the communication loss $\tilde{L}_{\text{comm}}(\alpha)$ we choose $\alpha = 1$ and we set $w_{\text{s}} = 0.7$.

The effects of the precoding are shown in Fig. 12. The vertical purple lines mark the direction of the main reflection servicing the UEs. The average total beam pattern is shown as well as the effects of the precoding vectors for each UE. The beam pattern for each UE shows a maximum towards its target direction and minimum towards the other UE. Both signals contribute to the illumination of the sensing area of interest. At the same SNR, the BER is similar for both UEs, as shown in Fig. 13. The beamforming gain is slightly lower for UE2, therefore we see a slightly higher BER. The BER is generally lower as in the other presented scenario, as QPSK instead of a higher order modulation is used.

VI. CONCLUSION

In this paper, we have proposed a novel loss function for end-to-end trainable JCAS systems based on supervised learning.

By separating the loss functions from the SNR, we have improved training convergence of our system together with its overall performance. We have compared a system with a 16QAM constellation to a geometrically shaped constellation. We observed similar behavior in terms of communication and sensing performance, and were able to adjust the trade-off between sensing and communication performance using the trade-off parameter w_{s}. The QAM constellation achieved comparable results for object detection and communication compared to the shaped constellation diagrams showing that JCAS systems can use legacy constellations. For AoA estimation, the shaped constellation achieves lower MSEs than QAM. The trained object detector and AoA estimator both outperform the respective baseline algorithms, namely a Neyman-Pearson-based power detector for object detection and ESPRIT for AoA estimation. By extending our setup, we demonstrate how spatial resources can be used to service multiple UEs.

In our future work, we want to build on our developed system and proof-of-concept to further explore the effects of multi-user MIMO and precoding in JCAS. To realize low-complexity solutions, we need to quantify the system complexity in comparison to classical algorithms and explore how reduction of the size of NN components affects the performance together with the expected performance-complexity trade-off. Paradigms such a model-based learning could help to find an appropriate structure of the trainable algorithms. We can integrate the analysis of this paper with our prior work on multiple target sensing in [11].

APPENDIX A CRB DERIVATION

We know from [16, Ch. 8.4] that the CRB for phase recovery of phase $\gamma = \pi \sin(\theta)$ is given by

$$C_{\text{CR}}(\gamma) = \frac{\sigma_{\text{n}}^2}{2N} \text{Re} \left\{ \left[S_{\text{f}} \left[\left(I + A^H A \frac{S_{\text{f}}}{\sigma_{\text{n}}^2} \right)^{-1} \left(A^H A \frac{S_{\text{f}}}{\sigma_{\text{n}}^2} \right) \right] \odot H^{\top} \right\}^{-1}. \quad (27)$$

In (27), N denotes the number of samples and σ_{n}^2 is the noise power. For the single source case, the signal spectral matrix S_{f} reduces to a scalar $s_{\text{f}} = \beta \sigma_{\text{s}}^2$, with transmit beamforming gain β and transmit power σ_{s}. The Matrix H is defined as

$$H = A_{\gamma}^H \left[I - A(A^H A)^{-1} A^H \right] A_{\gamma}, \quad (28)$$

with A_{γ} denoting the derivative of A with respect to γ. The steering matrix A simplifies for a uniform linear array to a steering vector

$$a = [1, \exp(-\text{j}\gamma), \exp(-\text{j}2\gamma), \ldots, \exp(-\text{j}(K-1)\gamma)]^{\top} \quad (29)$$

and the derivative a_{γ} with respect to γ to

$$a_{\gamma} = [1, -\text{j}\exp(-\text{j}\gamma), \ldots, -\text{j}(K-1)\exp(-\text{j}\gamma)]^{\top}. \quad (30)$$

For the CRB concerning the angle of arrival θ with γ being a function of θ, we can rewrite

$$\boldsymbol{C}_{\mathrm{CR}}(\gamma) = \boldsymbol{F}^{\top}\boldsymbol{C}_{\mathrm{CR}}(\theta)\boldsymbol{F}, \quad (\boldsymbol{F})_{i,j} = \frac{d\gamma}{d\theta}. \tag{31}$$

Evaluating the inner terms of (27) for one source/target yields:

$$\left(\boldsymbol{I} + \boldsymbol{A}^H\boldsymbol{A}\frac{\boldsymbol{S}_{\mathrm{f}}}{\sigma_{\mathrm{n}}^2}\right)^{-1} = \frac{\sigma_{\mathrm{n}}^2}{\sigma_{\mathrm{n}}^2 + K\beta\sigma_{\mathrm{s}}^2}, \tag{32}$$

$$\left(\boldsymbol{A}^H\boldsymbol{A}\frac{\boldsymbol{S}_{\mathrm{f}}}{\sigma_{\mathrm{n}}^2}\right) = \frac{K\beta\sigma_{\mathrm{s}}^2}{\sigma_{\mathrm{n}}^2}. \tag{33}$$

Now we calculate $\boldsymbol{H}$, which is also a scalar for the single source case:

$$H = \boldsymbol{a}_{\gamma}^H \left[\boldsymbol{I} - \boldsymbol{a}(\boldsymbol{a}^H\boldsymbol{a})^{-1}\boldsymbol{a}^H\right]\boldsymbol{a}_{\gamma} \tag{34}$$

$$= \boldsymbol{a}_{\gamma}^H\boldsymbol{a}_{\gamma} - \boldsymbol{a}_{\gamma}^H\boldsymbol{a}(\boldsymbol{a}^H\boldsymbol{a})^{-1}\boldsymbol{a}^H\boldsymbol{a}_{\gamma} \tag{35}$$

$$= \sum_{k=0}^{K-1} k^2 - \left(\sum_{k=0}^{K-1} k\right) \cdot \frac{1}{K} \cdot \left(\sum_{k=0}^{K-1} k\right) \tag{36}$$

$$= \frac{K(K-1)(2K-1)}{6} - \frac{K(K-1)^2}{4} \tag{37}$$

$$= \frac{K^3 - K}{12} = \frac{K(K^2-1)}{12}. \tag{38}$$

We can formulate the CRB concerning γ:

$$\boldsymbol{C}_{\mathrm{CR}}(\gamma) = \frac{\sigma_{\mathrm{n}}^2}{2N}\,\mathrm{Re}\left\{\left[\beta\sigma_{\mathrm{s}}^2\left[\frac{\sigma_{\mathrm{n}}^2}{\sigma_{\mathrm{n}}^2 + K\beta\sigma_{\mathrm{s}}^2}\frac{K\beta\sigma_{\mathrm{s}}^2}{\sigma_{\mathrm{n}}^2}\right]\right] \cdot \frac{K^3-K}{12}\right\}^{-1}. \tag{39}$$

Calculating the derivative of γ with respect to θ yields

$$\frac{\mathrm{d}\gamma}{\mathrm{d}\theta} = \frac{\mathrm{d}\pi\sin(\theta)}{\mathrm{d}\theta} \tag{40}$$

$$= \pi\cos(\theta). \tag{41}$$

Putting everything together yields (6).

APPENDIX B SUFFICIENT STATISTIC

In this section, we reason the use of correlation preprocessing in the sensing receiver by proving that it is a sufficient statistic for object detection and AoA estimation. A sufficient statistic is a set of values that contains all information of a set of measurement samples concerning the estimation of a certain parameter, i.e., an optimal estimator based on the sufficient statistic achieves the same estimation accuracy as an optimal estimator based on the measurement samples.

For AoA estimation, we can show the sufficiency mathematically following [21]. The log-likelihood function to esti-

mate the AoA θ of the measurement samples $\boldsymbol{Z}_{\mathrm{s}}$ can be written in an AWGN scenario as:

$$\log f_{\boldsymbol{Z}_{\mathrm{s}}}(\boldsymbol{Z}_{\mathrm{s}};\theta) = -KN_{\mathrm{win}}\log(\pi\sigma_{\mathrm{ns}}^2) - \frac{1}{\sigma_{\mathrm{ns}}^2}\sum_{n=1}^{N_{\mathrm{win}}}||\boldsymbol{z}_{\mathrm{s}}||^2$$
$$+ \frac{2\sqrt{N_{\mathrm{win}}}}{\sigma_{\mathrm{ns}}^2}\,\mathrm{Re}\left\{\alpha_{\mathrm{s}}\left(\boldsymbol{a}_{\mathrm{RX}}(\theta)\boldsymbol{a}_{\mathrm{TX}}(\theta)^{\top}\right)^H\boldsymbol{Z}_{\mathrm{s}}\boldsymbol{Y}^H\right\}$$
$$- \frac{|\alpha_{\mathrm{s}}|^2 N_{\mathrm{win}}}{\sigma_{\mathrm{ns}}^2}\boldsymbol{a}_{\mathrm{RX}}^H(\theta)\mathrm{Corr}(\boldsymbol{Y},\boldsymbol{Y})^H\boldsymbol{a}_{\mathrm{TX}}(\theta)\boldsymbol{a}_{\mathrm{RX}}^H(\theta)\boldsymbol{a}_{\mathrm{TX}}(\theta) \tag{42}$$

A sufficient statistic η can be found through the factorization theorem, i.e., by rewriting the log-likelihood as $\log f_{\boldsymbol{Z}_{\mathrm{s}}}(\boldsymbol{Z}_{\mathrm{s}};\theta) = f_1(\boldsymbol{Z}_{\mathrm{s}}) + f_2(\theta,\eta)$. According to [21], the sufficient statistic can be extracted as

$$\eta = \frac{1}{\sqrt{N_{\mathrm{win}}}}\boldsymbol{Z}_{\mathrm{s}}\boldsymbol{Y}^H. \tag{43}$$

In case $\boldsymbol{Y}$ is unknown, η can be approximated with the projection of the received signal on the signal space as in [22]:

$$\eta \approx \frac{1}{\sqrt{N_{\mathrm{win}}}}\boldsymbol{Z}_{\mathrm{s}}\left(\left(\boldsymbol{a}_{\mathrm{RX}}(\theta)\boldsymbol{a}_{\mathrm{TX}}(\theta)^{\top}\right)^{\dagger}\boldsymbol{Z}_{\mathrm{s}}\right)^H \tag{44}$$

$$= \frac{1}{\sqrt{N_{\mathrm{win}}}}\boldsymbol{Z}_{\mathrm{s}}\boldsymbol{Z}_{\mathrm{s}}^H\left(\left(\boldsymbol{a}_{\mathrm{RX}}(\theta)\boldsymbol{a}_{\mathrm{TX}}(\theta)^{\top}\right)^{\dagger}\right)^H, \tag{45}$$

with $(\cdot)^{\dagger}$ denoting the Moore-Penrose pseudoinverse. In our case, the transmit signal is known, but using the approximation (45) allows extension to bistatic scenarios, resulting in the approximated sufficient statistic

$$\tilde{\eta} = \mathrm{Corr}(\boldsymbol{Z}_{\mathrm{s}},\boldsymbol{Z}_{\mathrm{s}}). \tag{46}$$

Notably, the ESPRIT algorithm that we use as a baseline uses (46) as input. The comparison of the proposed algorithm and the baseline becomes more fair if both systems estimate based on the same statistic.

For object detection, the total power of the received signal projected on the AoAs is a sufficient statistic as shown in [21] and can be calculated from the correlation matrix in (43). Under an unknown transmit signal, the approximation in (45) applies. Therefore, we can feed (46) into the detection NN and approach optimal performance after training. The baseline NP-detector is also only based on the total power of the signal and does not rely on a known transmit signal.

REFERENCES

[1] C. Muth, B. Geiger, D. G. Gaviria, and L. Schmalen, "Loss design for single-carrier joint communication and neural network-based sensing," in *Proc. Workshop on Smart Antennas (WSA)*, Dresden, Germany, 2024.

[2] T. Wild, V. Braun, and H. Viswanathan, "Joint design of communication and sensing for beyond 5G and 6G systems," *IEEE Access*, vol. 9, pp. 30 845–30 857, Febr. 2021.

[3] J. M. Mateos-Ramos, J. Song, Y. Wu, C. Häger, M. F. Keskin, V. Yajnanarayana, and H. Wymeersch, "End-to-end learning for integrated sensing and communication," in *Proc. IEEE Int. Conf. Commun. (ICC)*, Seoul, Korea, 2022.

[4] J. M. Mateos-Ramos, C. Häger, M. F. Keskin, L. L. Magoarou, and H. Wymeersch, "Model-based end-to-end learning for multi-target integrated sensing and communication under hardware impairments," *IEEE Trans. Wireless Commun.*, pp. 1–1, Jan. 2025.

[5] S. Schieler, C. Schneider, C. Andrich, M. Döbereiner, J. Luo, A. Schwind, R. S. Thomä, and G. D. Galdo, "OFDM waveform for distributed radar sensing in automotive scenarios," *Int. J. Microw. Wireless Technol.*, vol. 12, no. 8, pp. 716–722, Jul. 2020.

[6] L. Giroto de Oliveira, D. Brunner, A. Diewald, C. Muth, L. Schmalen, T. Zwick, and B. Nuss, "Bistatic OFDM-based joint radar-communication: synchronization, data communication and sensing," in *Proc. European Microwave Week (EuMW)*, Berlin, Germany, Sep. 2023.

[7] T. O'Shea and J. Hoydis, "An introduction to deep learning for the physical layer," *IEEE Trans. Cogn. Commun. Netw.*, vol. 3, no. 4, Oct. 2017.

[8] S. Cammerer, F. Ait Aoudia, S. Dörner, M. Stark, J. Hoydis, and S. ten Brink, "Trainable communication systems: concepts and prototype," *IEEE Trans. Commun.*, vol. 68, no. 9, pp. 5489–5503, Jun. 2020.

[9] M. P. Jarabo-Amores, R. Gil-Pita, M. Rosa-Zurera, F. López-Ferreras, and R. Vicen-Bueno, "MLP-based radar detectors for Swerling 1 targets," in *Proc. Pattern Recognit. Image Analysis*, vol. 18, no. 1. St. Petersburg, Russia: Pleiades Publishing Ltd, 2008.

[10] J. Fuchs, A. Dubey, M. Lubke, R. Weigel, and F. Lurz, "Automotive radar interference mitigation using a convolutional autoencoder," in *Proc. IEEE Int. Radar Conf. (RADAR)*, Washington, DC, USA, 2020.

[11] C. Muth and L. Schmalen, "Autoencoder-based joint communication and sensing of multiple targets," in *Proc. Int. ITG Workshop Smart Antennas and Intl. Conf. Syst. Commun. Coding (WSA-SCC)*, Branschweig, Germany, Jan. 2023.

[12] C. Sturm and W. Wiesbeck, "Waveform design and signal processing aspects for fusion of wireless communications and radar sensing," *Proc. IEEE*, vol. 99, no. 7, pp. 1236–1259, May 2011.

[13] M. Braun, C. Sturm, and F. K. Jondral, "Maximum likelihood speed and distance estimation for OFDM radar," in *Proc. IEEE Radar Conf.*, Arlington, VA, USA, 2010.

[14] P. Swerling, "Probability of detection for fluctuating targets," *IEEE Trans. Inf. Theory*, vol. 6, no. 2, pp. 269–308, Apr. 1960.

[15] B. Geiger, F. Liu, S. Lu, A. Rode, and L. Schmalen, "Joint optimization of geometric and probabilistic constellation shaping for OFDM-ISAC systems," in *Proc. IEEE Int. Symposium Joint Commun. and Sensing*, Oulu, Finland, Jan. 2025, https://arxiv.org/abs/2501.11583.

[16] H. L. van Trees, *Optimum Array Processing: Part IV of Detection, Estimation, and Modulation Theory*. Wiley, 2002.

[17] A. Rode and L. Schmalen, "Optimization of geometric constellation shaping for Wiener phase noise channels with varying channel parameters," in *Proc. European Conf. on Optical Commun. (ECOC)*, Basel, CH, 2022.

[18] J. Li, A. Bose, and Y. Zhao, "Rayleigh flat fading channels' capacity," in *Proc. Commun. Netw. Services Res. Conf. (CNSR)*, Halifax, NS, Canada, 2005, pp. 214–217.

[19] D. P. Kingma and J. Ba, "Adam: A method for stochastic optimization," 2017, https://arxiv.org/abs/1412.6980.

[20] E. Castaneda, A. Silva, A. Gameiro, and M. Kountouris, "An overview on resource allocation techniques for multi-user MIMO systems," *IEEE Commun. Surveys Tuts.*, vol. 19, no. 1, pp. 239–284, Mar. 2017.

[21] I. Bekkerman and J. Tabrikian, "Target detection and localization using MIMO radars and sonars," *IEEE Trans. Signal Process.*, vol. 54, no. 10, pp. 3873–3883, Oct. 2006.

[22] I. Ziskind and M. Wax, "Maximum likelihood localization of multiple sources by alternating projection," *IEEE Trans. Acoust., Speech, Signal Process.*, vol. 36, no. 10, pp. 1553–1560, Oct. 1988.

BENEDIKT GEIGER (Graduate Student Member, IEEE) received the B.Sc. and M.Sc. degrees in electrical engineering and information technology from the Karlsruhe Institute of Technology (KIT), Karlsruhe, Germany, in 2020 and 2023, respectively, where he is currently working toward the Ph.D. degree. From 2021 to 2022, he was an ERASMUS+ Research Intern with the Optical Networks Group, University College London, London, U.K.. He wrote his master thesis with Nokia, Stuttgart, Germany, in 2022. His research interests include joint communication and sensing for 6G, ultra high-speed fiber optic communication systems, and the application of machine learning in communications. Mr. Geiger is a Student Member of the VDE, and his awards and honors include the first place of the Rohde & Schwarz Engineering Competition 2021. During his studies, he was a Scholar of the Konrad Adenauer Foundation, and is an alumnus of the Karlsruhe Institute of Technology's Leadership Talent Academy.

DANIEL GIL GAVIRIA (Graduate Student Member, IEEE) received the B.Sc. and M.Sc. degrees in electrical engineering and information technology from the Karlsruhe Institute of Technology (KIT), Karlsruhe, Germany, in 2018 and 2020, respectively, where he is currently pursuing the Ph.D. degree. He is also a Research and Teaching Assistant with the Communications Engineering Laboratory (CEL), KIT. His research interests include modern modulation schemes and signal processing for integrated sensing and communication (ISAC), specially in the context of automotive radar-communication and future cellular networks.

LAURENT SCHMALEN (S'07–M'13–SM'16–F'23) received the Dipl.-Ing. and Dr.-Ing. degrees in electrical engineering and information technology from RWTH Aachen University, Germany, in 2005 and 2011, respectively. From 2011 to 2019, he was with Alcatel-Lucent Bell Labs and Nokia Bell Labs. From 2014 to 2019, he was a Guest Lecturer with the University of Stuttgart, Stuttgart, Germany. Since 2019, he has been a Full Professor with Karlsruhe Institute of Technology, where he co-heads the Communications Engineering Laboratory. His research has been funded, among others, by the European Research Council (ERC) via an ERC Consolidator Grant. His research interests include channel coding, modulation formats, and optical communications. He was a recipient and a co-recipient of several awards, including the E-Plus Award for the Ph.D. thesis, the 2013 Best Student Paper Award from the IEEE Signal Processing Systems Workshop, the 2016 and 2018 Journal of Lightwave Technology Best Paper Awards, and the Bell Labs President Award. He serves as an Associate Editor for IEEE Transactions on Communications. He has served as TPC member for most major conferences in the fields of communications and information theory.

CHARLOTTE MUTH (Graduate Student Member, IEEE) received the B.Sc. and M.Sc. degrees in electrical engineering and information technology in 2019 and 2021, respectively from the Karlsruhe Institute of Technology, Karlsruhe, Germany. She is currently pursuing a Ph.D. at the Communications Engineering Lab at Karlsruhe Institute of Technology. Her research interests include the integration of sensing into communication systems, signal processing, and estimation using trainable algorithms and technologies for wireless communication. Ms. Muth has been part of the Executive Committee of the IEEE Student Branch at Karlsruhe Institute of Technology since 2022.

• • •